

Investigation of fuel volatility on the heat transfer dynamics on piston surface due to the pulsed spray impingement

Zhi-Fu Zhou^{a*}, Lin Liang^a, Safwan Hanis Mohd Murad^b, Joseph Camm^c, Martin Davy^{b*}

^aState Key Laboratory of Multiphase Flow in Power Engineering, Xi'an Jiaotong University, Xi'an 710049, China

^bDepartment of Engineering Science, University of Oxford, Oxford OX1 3PJ, UK

^cSchool of Engineering, Technology and Design, Canterbury Christ Church University, Canterbury CT1 1QU, UK

Corresponding author: zfzhou@mail.xjtu.edu.cn; martin.davy@eng.ox.ac.uk

Abstract

The fuel spray in a gasoline direct injection (GDI) engine can impinge on the piston surface to form a liquid film, which leads to a decrease of the combustion efficiency and the increase of particulate emissions. The dynamic heat transfer process resulting from the impingement has an important effect on the evaporation of the liquid film and its residence time. In this study, two pure component fuels (methanol and n-pentane), and three fuel blends with different initial boiling points and enthalpies of vaporization marked as Fuel B, Fuel C and Fuel D, are designed to investigate the effect of the fuel volatility on heat transfer dynamics of pulsed spray impingement with different: injection temperatures (T_{inj}), injection pressures (P_{inj}), piston temperatures (T_{pis}) and injection distances (D_{inj}). The results show that the spray a transient heat transfer induced by different fuel sprays are very sensitive to changes of T_{inj} and D_{inj} , and also depend on their boiling points and enthalpies of vaporization. The impinging and cooling intensities are greatly reduced when the pressure ratio of ambient pressure to saturation pressure (P_a/P_{sat}) decreases, as a result of increasing T_{inj} . The maximum surface temperature drop ($\Delta T_{s, max}$) and peak heat flux (q_{max}) on the impinging surface are reduced greatly by over 60% for fuels with low enthalpy of vaporization such as n-pentane, Fuel B, Fuel C and Fuel D, while they are only reduced by less than 15% for methanol with highest enthalpy of vaporization when T_{inj} increases from 25 °C to 140 °C. Exponential equations are proposed to describe the relationship between q_{max} and P_a/P_{sat} . When D_{inj} increases from 50 mm to 70 mm, q_{max} is reduced by over 10% for fuels such as n-pentane, methanol, Fuel B and Fuel C with low initial boiling points, whereas q_{max} is increased slightly by 7% for Fuel D with the highest boiling point. On the other hand, the transient heat transfer of different fuels present similar trends in response to the changes of P_{inj} and T_{pis} . $\Delta T_{s, max}$ and q_{max} nearly present a linear variation with P_{inj} and T_{pis} for all fuels.

Key word: spray impingement, fuel volatility, transient heat transfer, GDI engine, flash boiling

1. Introduction

Because of its high compression ratio, high intake volumetric efficiency and good fuel economy, gasoline direct injection (GDI) engines are replacing port fuel injection (PFI) engines as the preferred power unit for internal combustion engine powered equipment. However, the limited cylinder space with GDI may easily lead to the phenomenon of wall wetting on the piston crown and cylinder wall due to spray impingement, which lowers the combustion efficiency and increases the level of hydrocarbon and particulate matter emissions significantly [1-3]. Currently, with requirements on emissions for health and environmental protection becoming increasingly stringent, fuel impingement and its consequent wall wetting have been subject to increased attention [4, 5].

With the development of engine technology and the emergence of new mixture formation methods, the liquid film formed on piston surface or cylinder wall due to the fuel spray impingement is mitigated to some extent. Increasing fuel injection temperature to promote flash boiling is considered as a promising approach to improve fuel atomization and reduce emissions [6, 7]. However, no matter whether the strategy is for a homogeneous or stratified mixture, the phenomenon of liquid film formation is still common in direct injection engines due to the increase of injection pressure and the strategy of early injection [8]. The fuel spray impingement on the wall will produce a strong instantaneous cooling effect, resulting in a sharp drop in the wall temperature and a dramatic increase in heat flux, and will further negatively affect the mixing and combustion process of oil and gas in the combustion chamber. This dynamic heat transfer is believed as one of the most important factors that determines liquid film formation and its evaporation lifetime [9-11].

Over the years, researches on the spray-wall interaction in GDI engine have been widely studied, but most focus on the atomization and its impinging morphology [12-14]. Only a few scholars have studied the dynamic heat transfer on piston surface from the fuel spray impinging the wall. Serras-Pereira et al. [15, 16] investigated the influences of fuel types, engine temperature and injection strategy on heat flux variation on the surface exposed to the spray impingement with a fast-response heat flux sensor. The results showed that the heat flux produced by the impingement was closely related to the type of fuel and the injection temperature. In order to reduce the impingement on the engine liner, an injection strategy with multiple injections was proposed. Kopple et al. [17] employed a 0.3 mm-thick embedded fast-response thermocouple to record the temperature drop on the piston surface caused by fuel impingement under different working conditions such as: spray pressure, engine load and speed. The results showed that the higher the injection pressure, the faster the piston surface temperature dropped. The amount of particulate matter emission can be reduced due to less liquid film being formed on the wall. Leonard et al. [18] investigated the changes in the lifetime of the fuel film attached to a heated metal plate at different temperatures. The results indicated that a higher surface

temperature of the metal plate could enhance the shrinking and vaporizing rates of the liquid film significantly. When the temperature reached 130 ~ 180 °C, strong nucleate boiling phenomenon occurred, which resulted in a quick disappearance of the liquid film. Lepperhoff et al. [19] and Hsieh et al. [20] observed film boiling at surface temperatures beyond the Leidenfrost point. The presence of the gas film hindered the direct contact between the liquid film and the wall surface, which was favorable towards reducing the carbon deposits. Tang et al. [21] conducted an optical study of spray-wall impingement to investigate the ignition, flame development and unburned hydrocarbon (UHC) emissions in a light-duty optical engine, revealing that fuel injection time had great effect on liquid film formation, combustion efficiency and UHC emissions.

In recent years, methanol and ethanol fuels have been widely used as an alternative fuel with higher oxygen content, higher octane number and lower boiling point [22]. In addition, methanol has been widely championed as clean burning made from alternative non-petroleum energy sources and as such, the behavior of methanol-gasoline blends are of substantial current interest to the automotive industry. Liu et al. [23] investigated the effects of three kinds of oxygenated fuel blends i.e., ethanol-gasoline, n-butanol-gasoline, and 2,5-dimethylfuran (DMF)-gasoline-on fuel consumption, emissions, and acceleration performance. It is found that the particle number (PN) emissions were significantly decreased when using the high blending ratios of the three kinds of oxygenated fuels while the addition of butanol and ethanol reduces NO_x emissions additionally. Aleiferis and Romunde [16, 24] studied the effect of physical properties on the atomization and spray formation under hot fuel conditions using iso-octane, n-pentane, gasoline, ethanol and n-butanol through high speed imaging and droplet sizing techniques. It was found that the volatility influenced the spray penetration, spray angle and droplet size greatly. *n*-Pentane with highest volatility was more prone to collapse. Meanwhile, its spray cone angle was smaller than gasoline, and the Sauter mean diameter (SMD) was the smallest. Qian et al. [25] also found that fuel volatility had significant influence on combustion and emissions for GDI engine through testing five real distillate gasoline fuels with different 50%v distillation temperatures (The temperature at which the recovered distilled condensate occupies 50% of the volume of the original liquid); increasing the fuel volatility could improve the fuel economy and particulate matter (PM) emissions. Vanderwege and Hochgreb [26] investigated the effect of fuel volatility on spray distribution in direct-injection gasoline engine with a high-pressure swirl injector. The results showed that flash boiling of volatile components in the fuel led to a change from the hollow-cone structure to a solid-cone distribution under warmed-up conditions and low intake pressure, and a 40% decrease in droplet diameter. Tong et al. [27] experimentally investigated the effects of gasoline component volatility on gasoline direct injection (GDI) engine cold start. The results showed that the increased wall wetting reduced the equivalence ratio, causing the poor cold start performance observed with the

low volatility fuel blend, while the high volatility fuel component improved engine performance and reduced the number of cycles required to attain stable combustion.

As can be seen from the above, fuel volatility is crucial to GDI engine performance. It influences fuel spray angle, spray structure, penetration distance and subsequent spray interaction with the piston surface or cylinder wall. During the highly transient and complex process of spray impingement, the heat transfer behavior determines the liquid film formation, evaporation and residence time, consequently affecting the fuel combustion efficiency and PM emission level. This study aims at investigating the effect of fuel volatility on the heat transfer dynamics during the highly transient process of a pulsed spray impinging on a surrogate piston surface. Five types of fuel, including two single component fuels (n-pentane, methanol), and three fuel blends with different boiling points and enthalpies of vaporization have been examined for different: injection temperatures, pressures, piston temperatures and impingement distances. Spray and impinging morphology are recorded through a high speed camera. A fast response platinum resistance thermometer array is used to record the rapid change of surface temperature and an unsteady heat conduction analysis is used to estimate the heat flux.

2. Experimental setup and measurement methods

2.1 Experimental system

Figure 1 shows a schematic of the experimental system, and Fig. 2 shows the photograph of the experimental set-up. The fuel is drawn from a syringe and pressurized through a stepped-piston intensifier to give a fixed pressure ratio using compressed nitrogen, which can provide a maximum fuel pressure of 30 MPa. The injector is a modified Jaguar Land Rover AJ133 engine six-hole nozzle spray injector. Five of the holes have been sealed leaving only one hole for injection. The injector is located at the top center of the spray chamber with an appropriate angle to make the single spray plume impinge the horizontal piston surface vertically. The injector is embedded in a heating block with four heaters, and the injector temperature is controlled by a LabVIEW system using PID temperature feedback control. A surrogate piston made of copper is located at the bottom center of the chamber, with 7 internal holes for heater elements insertions. The piston is insulated except for the top surface which is exposed to the fuel impingement, and its temperature can be heated to the designed value under the control of another LabVIEW system. The spray chamber is made of a full-length optical cylinder liner with an inner diameter of 89 mm, and is open to the atmosphere at the top and the exhaust air is drawn out through extraction system at the bottom. More details about the whole system can be found in our previous study [28].

A Photron Fastcam 1024 PCI camera is used to visualize the spray. Mie scattering spray images are taken at 4500 frames per second using an f/1.2 lens with illumination from a 100W LED array. The

136 exposure is set to 3.30 μs to capture as much transient detail of the spray as possible.

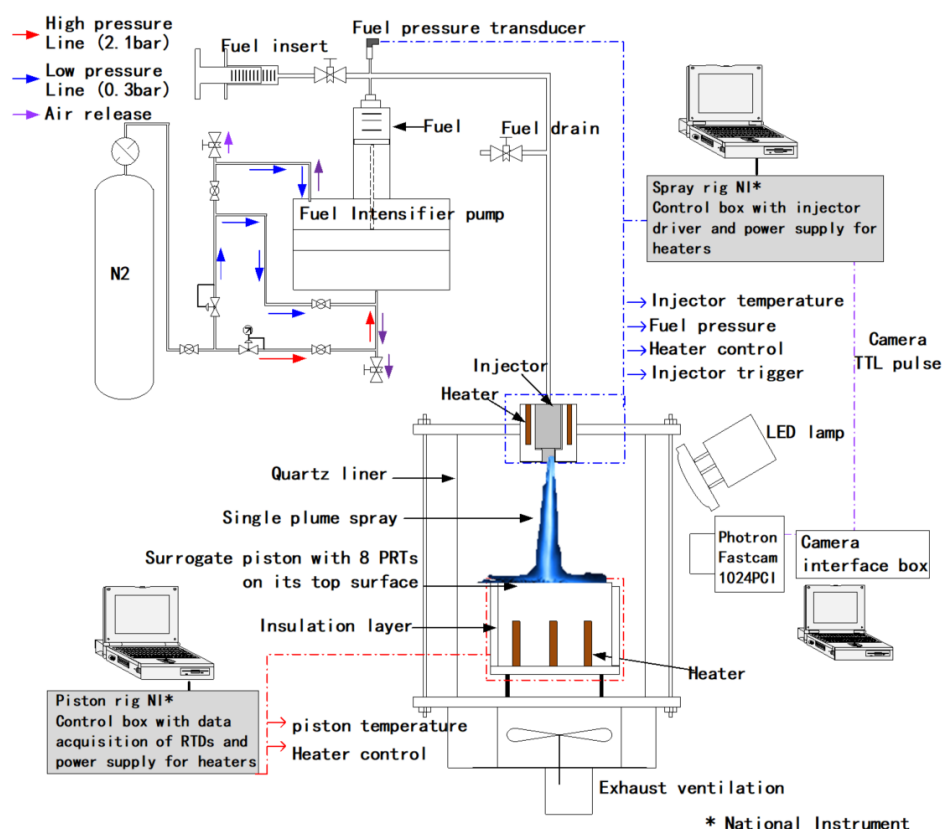


Fig. 1 Schematic of the experimental system [28]

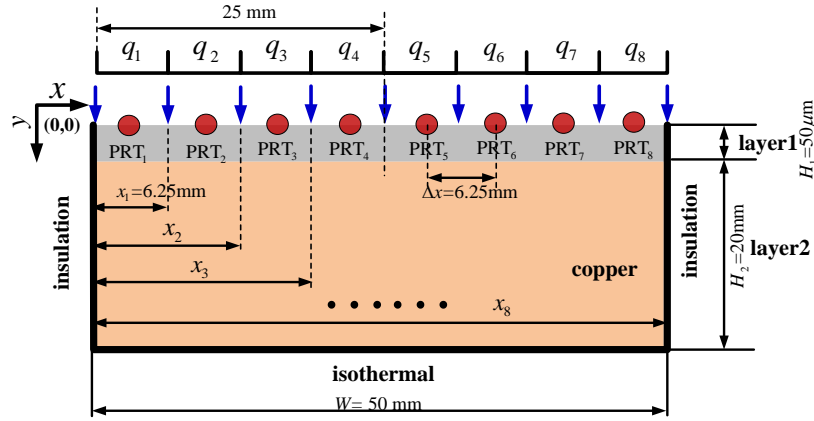


Fig.2 Photograph of experimental set-up

2.2 Surface transient temperature measurement and heat flux calculation

A fast-response thin film platinum resistance thermometer (PRT) array with a thickness of 0.5 μm is used to measure the surface temperature change. 8 PRTs fabricated onto a strip of thin flexible 50 μm polyimide insulating layer (Upilex) is attached to the top surface of the surrogate piston to measure

the surface temperature (please see Fig.2). According to the surrogate piston design and the PRT arrangement, the geometry model for a two dimensional heat flux calculation is shown in Fig. 3. The model is composed by two layers. Layer 1 is an insulating layer (Upilex, $H_1 = 50 \mu\text{m}$) on the top surface of which the thin PRTs are deposited. Layer 2 is the copper ($H_2 = 20 \text{ mm}$) of the surrogate piston. The thickness of the PRTs ($0.5 \mu\text{m}$) can be neglected since it is far smaller than those of the two other layers. Thus, the temperature measured by the PRTs can be directly regarded as the surface temperature of Layer 1 in the heat flux calculation.



154

155 **Fig.3** Geometry model of the two-layer system for solution of the Inverse Heat Conduction problem (IHCP) with
156 the PRTs [28]

157 Before the experiment, careful calibration of the eight PRTs yields correlations between the
158 temperature and voltage acquired by the NI-DAQ system. In the experimental system, there is a pulse
159 signal controlled by a manual switch that is used to synchronize the: the fuel injection event, the high
160 speed camera and the temperature data acquisition. The sampling rate of the temperature data is 100
161 kHz.

162 In the direct heat conduction problem, the temperature distribution can be solved directly by the
163 known surface heat flux. However, when the surface heat flux is unknown and the temperature at a
164 certain location is measured, it is the inverse heat conduction problems (IHCP). The IHCP solution is
165 developed based on the minimization of the errors between estimated and measured temperatures.
166 More details of temperature measurement and heat flux calculation can be found in our previous study
167 [28, 29].
168

2.3 Fuel properties

The fuels tested in this study were selected in order to advance understanding of the effect of fuel volatility on heat transfer and mixture preparation in GDI engines. The five fuels tested included two pure component fuels (n-pentane and methanol), and three multi-component fuels, M15P45D7U5T28 (Fuel B), M15ISO45T28D7U5 (Fuel C) and ISO55P5T28D7U5 (Fuel D) were examined. The composition and physical properties of various fuels are shown in Table 1 in which the enthalpies are calculated based on the NIST-REFPROP database. Their modelled distillation curves are shown in Fig.4 [30].

The three fuel blends are all heavy-end fuels which were modelled to have similar T90 distillation values but to vary in their T50 values as shown in Fig. 4. The heavy component used in all three fuels comprised of 28% toluene, 5% n-undecane and 7% n-decane. Fuel B and Fuel C are two kinds of M15 methanol/gasoline blend with different components, while Fuel D is a gasoline-like fuel (without methanol). The fuel blends are designed based on the European Standards - EN228 E100, which requires that the distillation curve where evaporation must lie within the range of 46% to 71% of total evaporated volume at a temperature of 100 °C (375.15K).

Among the five fuels, n-pentane has the lowest boiling point and second smallest enthalpy of vaporization, thus having the highest volatility. Methanol has a low saturated vapor pressure and the highest enthalpy of vaporization. The physical properties of the multi-component fuel have changed greatly compared with the original pure material. Fuel B and fuel C have lower initial boiling points due to the addition of methanol compared with fuel D without methanol, which makes them have higher volatility and more prone to flash boiling at the initial stage. On the other hand, methanol has the highest enthalpy of vaporization. This means that methanol has to absorb the largest amount of heat and is most difficult to evaporate completely during the vaporizing stages if the liquid film forms on the piston surface. In addition, the difference in evaporation between fuel B and fuel C is mainly due to the amount of n-pentane. Fuel B is more volatile as it contains 45% n-pentane while fuel C contains no n-pentane but 45% iso-octane. At the end of the distillation process, the distillation curves of the three multi-component fuels overlap because that only the aromatic hydrocarbon is left.

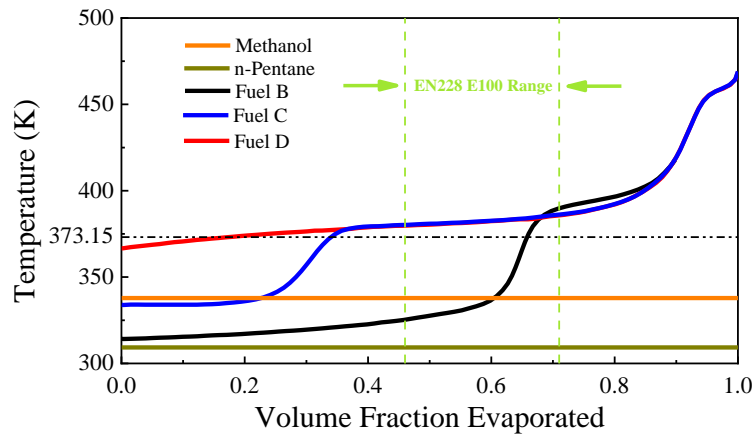


Fig.4 Modelled distillation curves for 5 fuels. Note that the curves track a temperature trajectory required to give fuel vapour pressure of 1.013 bar and therefore do not directly reflect the ASTM D86 procedure in the early stages of distillation as no account is taken of dissolved gases and no liquid is evaporated until the vapor pressure reaches 1.013 bar [30]

Table 1 Physical properties of 5 fuels

	n-Pentane	Methanol	Fuel B (M15P45D7U5T28)	Fuel C (M15ISO45T28D7U5)	Fuel D (ISO55P5T28D7U5)
Methanol Vol (%)	—	100	15	15	—
n-Pentane Vol (%)	100	—	45	—	5
Iso-octane Vol (%)	—	—	—	45	55
n-Decane Vol (%)	—	—	7	7	7
Undecane Vol (%)	—	—	5	5	5
Toluene Vol (%)	—	—	28	28	28
Enthalpy of Vaporization at 1 atm (kJ/kg)	358.26	1101.07	575.01	709.95	352.41

2.4 Experimental uncertainty analysis

The repeatability of the experiment is carefully examined through multi experimental tests. During three measurements of surface temperature at the same injection conditions, it is noticed that all the three temperature curves are close to each other (nearly overlap). The standard deviations are quite small, most of which in the measurement range of (10, 000 data points in acquired in 1 s) were less than 1 K. As a result, the heat flux based on the surface temperature data also has good repeatability, little deviation from their average value for each curve during the three experiments. And the time (t_{\max}) when heat flux reaches its peak value takes place at the same time.

As for the experimental error, the PRTs have been calibrated against an ASTM mercury-in-glass

distillation thermometer with a resolution of 0.2 K; such thermometers are typically accurate to better than ± 0.2 K. Any drift in the Wheatstone bridge balance will not be important as heat flux is derived from the rate of change of temperature. In the following results, we do not show the error bars because of too many points for all the curves and the quite small uncertainty.

3 Results and discussions

3.1 Spray images

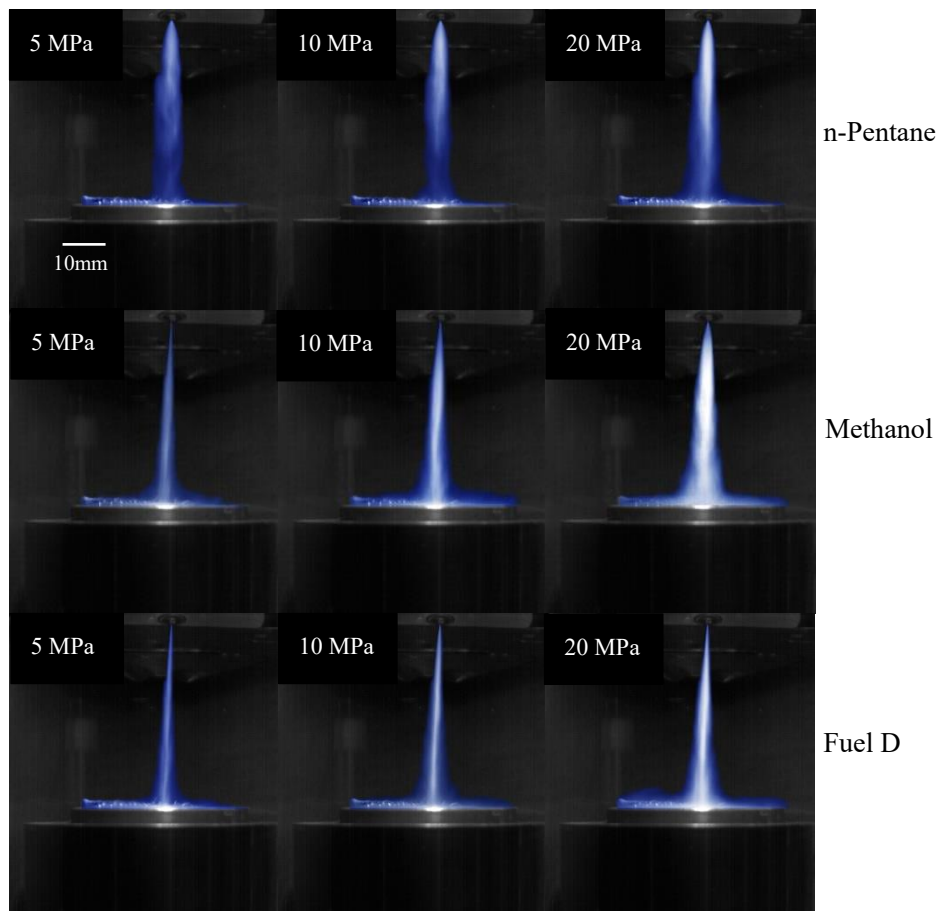
Fig. 5 presents images of a single spray plume and its impingement on the piston surface from one hole of the injector at different injection pressures of n-pentane, methanol and fuel D, where piston surface temperature, injection temperature and spray distance are 90 °C, 110°C and 50 mm, respectively. As the injection pressure increases, the spray becomes dense and the cone angle increases. This is because the higher injection pressure causes the fuel to eject out of the nozzle at greater speed and in greater quantity, which strengthens the interaction of the fuel with the atmosphere, thereby increasing the spray angle and width. Meanwhile, the spray impinging intensity increases with injection pressure, causing more droplets to rebound after impinging the wall. This is likely to reduce the droplets sticking to the piston surface, and thus shorten the existence time of liquid film [31].

From further observation of the spray morphologies for different fuels, it is found that they show different sensitivity to the change of injection pressure. Fuel D is obviously less influenced by the pressure change compared with n-pentane and methanol. It always shows a jet-like spray under different pressures. This can be explained by the fact that fuel D with iso-octane as the main component maintains the highest initial boiling point of 93 °C, thus the injection temperature is not high enough to induce flash boiling in the spray. However, flash boiling behaviour can be observed for the n-pentane and methanol sprays due to the fuel's boiling points being much lower than the injection temperature.

Fig. 6 presents the images of single spray plume and its impingement on the piston surface from one hole of the injector at different injection temperatures for the same three fuels, where piston surface temperature, injection pressure and spray distance are 90 °C, 10 MPa and 50 mm, respectively. Five injection temperatures from 25 °C to 140 °C have been tested. At the injection temperatures below their boiling points and a little above their boiling points (within 20 K), all three fuels present the same jet-like spray with a high fuel concentration that produces an intense **impingement** on the piston surface at the jet center. Fuel volatility has little effect on spray morphology at the non-flash boiling condition.

With the increase of injection temperature, the pressure ratio of the back pressure to the saturated vapor pressure (P_a/P_{sat}) gradually decreases. When the temperature rises to 80, 110 and 140 °C (above their boiling points ~ 45 °C) for n-Pentane, methanol and fuel D respectively, corresponding to the pressure ratio of about 0.35, a flash boiling spray can be observed with larger spray width and angle.

247 This observation is consistent with the conclusion made by Zeng et al. and Zhang et al. [32, 33]. That
 248 is they defined the fuel spray into three distinct regions: non flash-boiling ($P_a/P_{sat} > 1$), transitional
 249 flash-boiling ($0.3 < P_a/P_{sat} < 1$) and flare flash-boiling conditions ($P_a/P_{sat} < 0.3$) with the increasing of
 250 superheat degree. The atomization mechanism transitions from depending on the dynamic forces
 251 acting on the liquid surface, to a bubble formation and expansion phenomena at the condition of P_a/P_{sat}
 252 < 1 . The flash boiling process is accompanied by the nucleation, growth and collapse of bubbles, which
 253 makes the spray more violent leading to larger spray width and angle [34, 35]. Further increase of the
 254 injection temperature causes larger difference among the spray morphologies and interactions with
 255 piston surface for different fuels. For n-pentane, there are no increases in the spray angle and width.
 256 However, the spray concentration is diluted and the spray impinging on piston surface is weakened
 257 greatly at high level of superheat, e.g., the spray even disappears at the far downstream region and it
 258 cannot reach the piston surface with a 140 °C injection temperature. This is because n-pentane has the
 259 lowest boiling point, highest volatility and very low enthalpy of vaporization, thus flash boiling is most
 260 likely to occur with the largest evaporation rate and shortest lifetime of droplets within the spray. For
 261 methanol, a further increase of injection temperature to 140 °C leads to a continuous increase in spray
 262 angle and width, and a larger interaction area between spray and piston surface.



263

Fig. 5 Effect of injection pressure on spray and its impingement at conditions of $D_{inj}=50$ mm, $T_{inj}=110$ °C, $T_{pis}=90$ °C

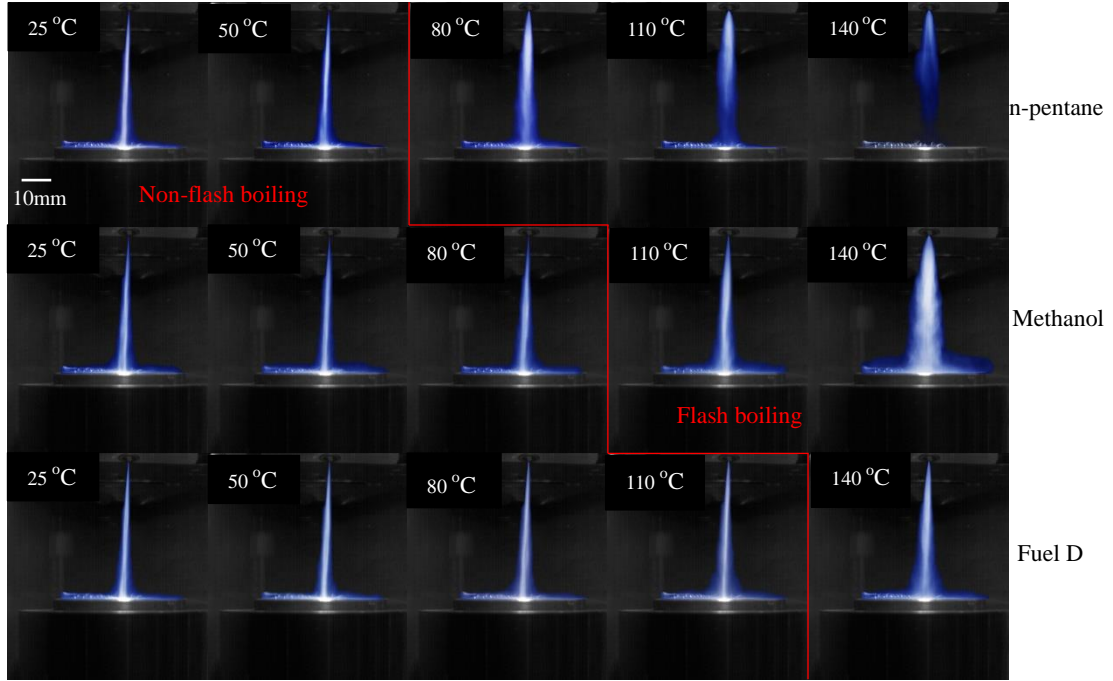


Fig. 6 Effect of injection temperature on spray and its impingement at conditions of $D_{inj}=50$ mm, $P_{inj}=10$ MPa, $T_{pis}=90$ °C

3.2 Surface heat transfer dynamics

The most central measurement point exposed to the spray impingement (PRT5 shown in Fig. 3) experienced the most obvious temperature change due to the most intense **impingement** during the transient heat transfer process compared with other measurement points (The typical 8 transient temperature curves were shown in Fig. 5 of the previous work [28]). Therefore, the temperature and heat flux from this measurement point were selected as the salient value in the following subsections to illustrate the effects of injection temperature (T_{inj}), injection pressure (P_{inj}), piston temperature (T_{pis}) and injection distance (D_{inj}) on the transient heat transfer behavior of the piston surface for the different fuels. The duration of each injection event was set as 2 ms for all experiments.

3.2.1 Effect of fuel injection temperature

Fig. 7 and Fig. 8 show the variations of surface temperature and heat flux with time for the 5 fuels at two injection temperatures (low $T_{inj} = 25$ °C and high $T_{inj} = 140$ °C), at constant impingement distance, piston temperature and injection temperature, $D_{inj} = 50$ mm, $T_{pis} = 90$ °C and $P_{inj} = 10$ MPa. As can be seen from Figs 7 and 8, the surface temperature of the piston drops rapidly after being hit by the fuel at both high and low injection temperatures. The temperature drop lasts for about 2 ms, which is equal

to the injection duration. After that, the piston surface temperature starts to rise at a slower rate compared with when it was being cooled. Correspondingly, after a rapid growth process, the heat flux reaches its peak. It then declines rapidly and follows a slow decreasing period until the liquid film is completely evaporated. The rapid temperature decrease and heat flux increase at the first stage are attributed to the strong cooling effect mainly due to the intense impingement of fuel droplets, while the following stage of gradual temperature increase and heat flux decrease are caused by the evaporative cooling of the liquid film formed on piston surface. Finally, the surface temperature will return to the initial value and the heat flux goes to zero once the liquid film disappears because of its complete evaporation.

To better present the sensitivity of transient heat transfer to fuel volatility, Fig. 9 shows the variations of peak heat flux (q_{\max}) and maximum surface temperature drop ($\Delta T_{s, \max}$) with injection temperature for 5 fuels. It can be found that, $\Delta T_{s, \max}$ and q_{\max} present a continuous decreasing with increasing T_{inj} , although they are less decreased for methanol than other fuels. Even when the fuel temperature exceeds the piston surface temperature, a drop in temperature is still observed on the piston surface because of the impingement of spray droplets and violent vaporizing at the piston surface. When the fuel injection temperature increases from 25 °C to 140 °C, $\Delta T_{s, \max}$ is reduced by 14.48%, 92.08%, 78.69%, 59.27% and 60.77%, and q_{\max} is reduced by 11.61%, 94.71%, 77.20%, 56.98% and 61.48% for methanol, n-pentane, fuel B, fuel C and fuel D respectively.

At the low injection temperature ($T_{\text{inj}} = 25$ °C), all fuel sprays produce a strong impingement on the piston surface, leading to large $\Delta T_{s, \max}$ and q_{\max} due to the strong convective heat transfer between the droplets and piston surface. The droplets of n-pentane evaporate most easily and consequently produce the lowest droplet temperature before reaching the piston surface due to the lowest boiling point and highest volatility, thus n-pentane spray causes the largest $\Delta T_{s, \max}$ and q_{\max} . Fuel D possesses the lowest $T_{s, \max}$ and q_{\max} because of its highest initial boiling point. When the injection temperature rises from 25 °C to 140 °C, the results change a lot. The droplets of n-pentane and fuel B with lowest boiling points evaporate substantially during flight, greatly reducing the liquid impingement on the piston surface as evidenced in Fig.6. As a result, their $\Delta T_{s, \max}$ and q_{\max} decrease most heavily. However, $\Delta T_{s, \max}$ and q_{\max} change little for methanol. Methanol spray still causes very strong cooling effect on the piston surface at high T_{inj} of 140 °C. This is mainly because of its far larger enthalpy of vaporization compared with other fuels. This means that the droplets need to absorb a lot of heat to evaporate completely, and this cannot be provided by heat transfer from the ambient gas. As a result, a large number of droplets can impinge the piston surface and cause a strong cooling effect even if the injection temperature is high. In addition, the liquid film is easy to form and difficult to evaporate due to the

largest latent heat, which is bad for the emission of particulate matter of GDI engines. This phenomenon is also reflected to a certain extent with fuel C, which contains 15% methanol with the second largest enthalpy of vaporization.

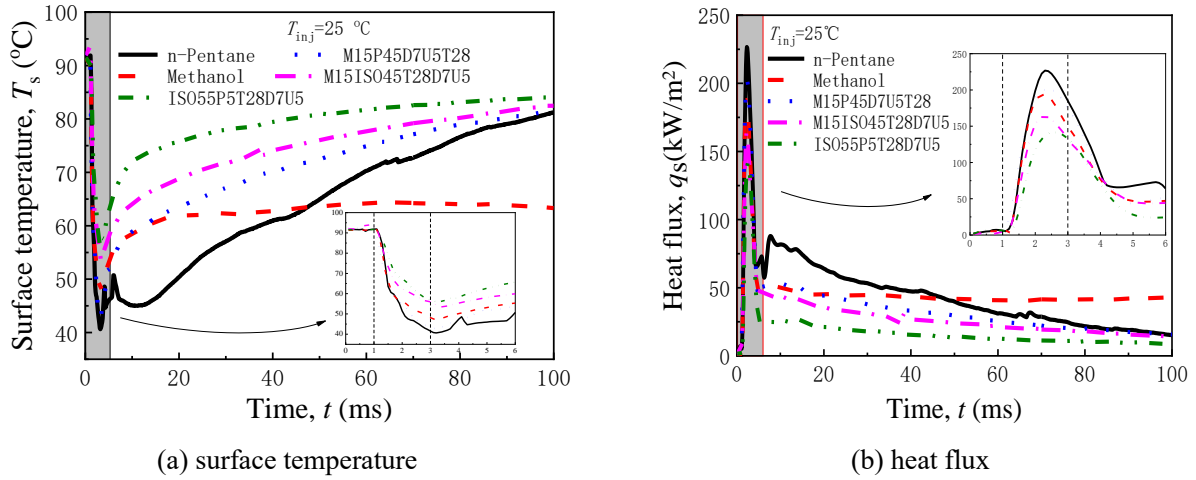


Fig.7 Variation of (a) surface temperature and (b) heat flux as a function of time at the condition of $T_{inj}=25^\circ\text{C}$, $D_{inj}=50\text{ mm}$, $T_{pis}=90^\circ\text{C}$, $P_{inj}=10\text{ MPa}$

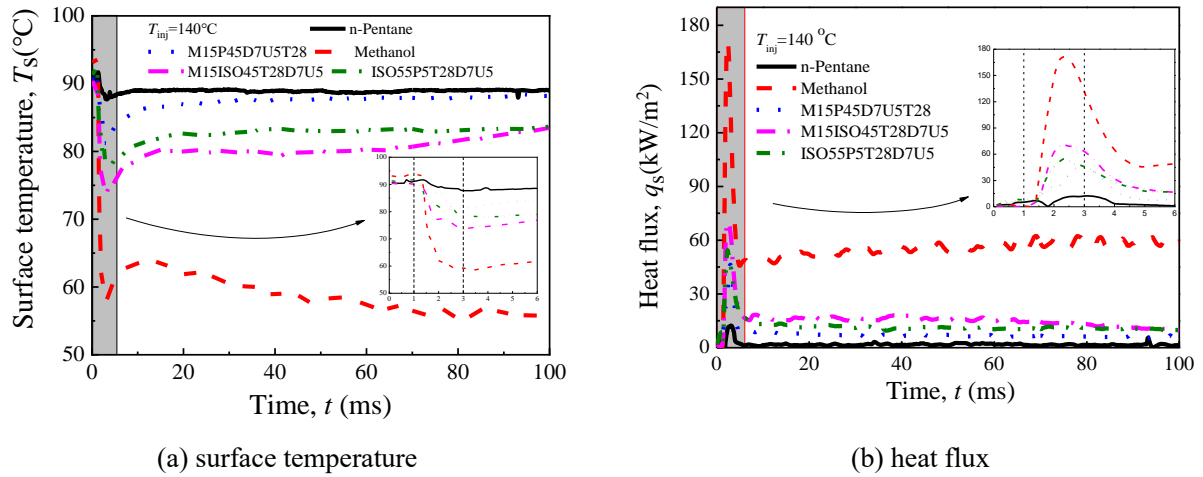


Fig.8 Variation of (a) surface temperature and (b) heat flux as a function of time at the condition of $T_{inj}=140^\circ\text{C}$, $D_{inj}=50\text{ mm}$, $T_{pis}=90^\circ\text{C}$, $P_{inj}=10\text{ MPa}$

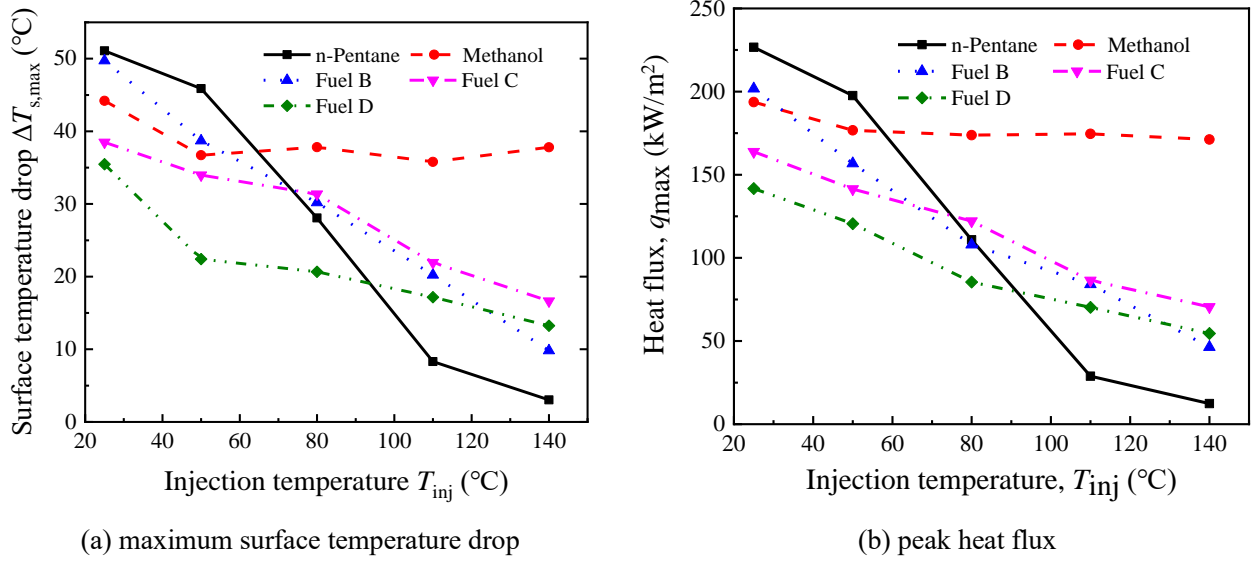
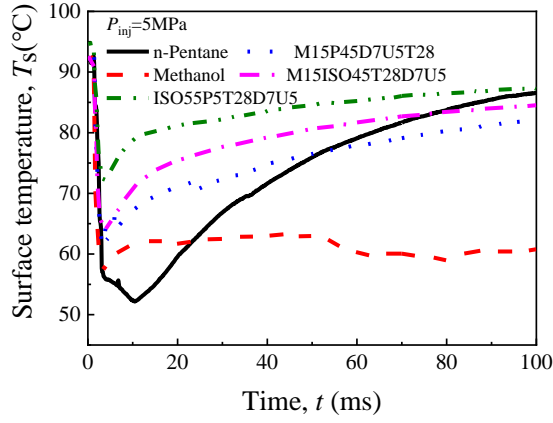


Fig.9 Variations of maximum surface temperature drop ($\Delta T_{s,max}$) and (b) peak heat flux (q_{max}) with injection temperature at the condition of $D_{inj}=50$ mm, $T_{pis}=90$ °C, $P_{inj}=10$ MPa

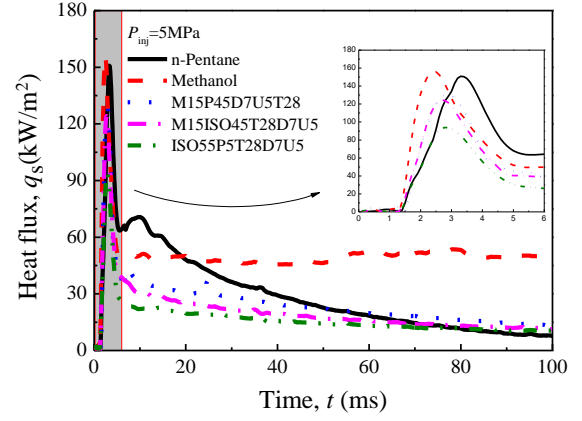
3.2.2 Effect of injection pressure

Fig. 10 and Fig. 11 show the changes in surface temperature and heat flux with time for the 5 fuels at two injection pressure (low $P_{inj} = 5$ MPa and high $P_{inj} = 20$ MPa), while other conditions are the same, $D_{inj}= 50$ mm, $T_{pis} = 90$ °C and $T_{inj}=50$ °C. The results show that a larger P_{inj} brings lower T_s , higher q_s and a shorter liquid lifetime. This can be explained by three contributions. Firstly, droplets from the higher-pressure nozzle impinge the piston surface with a higher velocity, which enhances the heat transfer and reduces liquid film lifetime. Secondly, at the same duration of injection, more fuel will be ejected at larger pressure accompanied by larger number of droplets, also leading to a stronger cooling effect on the piston surface. Thirdly, as shown in Fig. 5, droplets with a high speed are more likely to splash instead of adhering to the surface, which reduces the duration of the liquid film.

Fig. 12 shows the variations of $\Delta T_{s,max}$ and q_{max} with injection pressure. It is observed that $\Delta T_{s,max}$ and q_{max} increase monotonically with P_{inj} because of the increasing impingement intensity. All fuels present a quite similar trend of heat transfer behavior at the low and high injection pressures. That is, fuels with a low initial boiling point or high enthalpy of vaporization cause relatively large surface temperature drop and heat flux on the piston surface. The explanation can refer to the last section of 3.2.1 for the case of heat transfer of fuels at low injection temperature. Therefore, unlike with a change of injection temperature, the transient heat transfer of different fuels is relatively insensitive to a change of injection pressure.

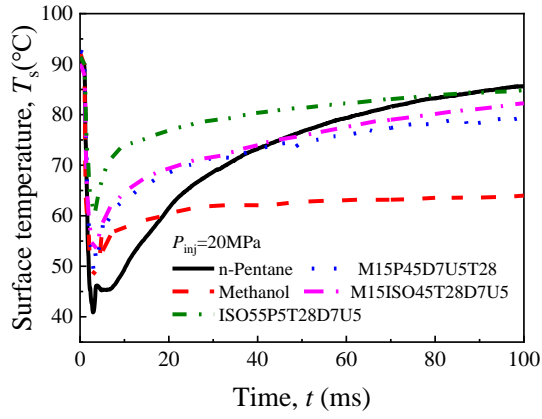


(a) surface temperature

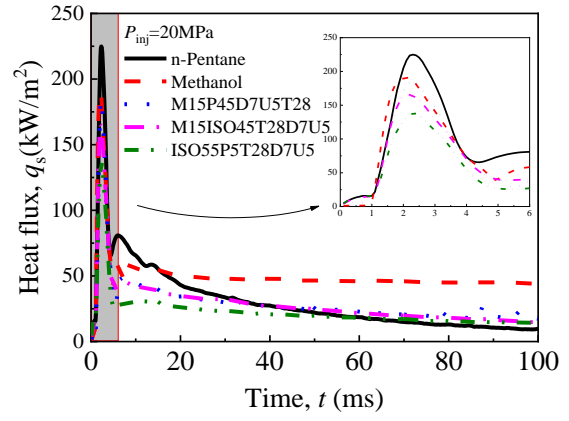


(b) heat flux

Fig.10 Variation of (a) surface temperature and (b) heat flux as a function of time at the condition of $P_{inj}=5$ MPa, $D_{inj}=50$ mm, $T_{pis}=90$ °C, $T_{inj}=50$ °C

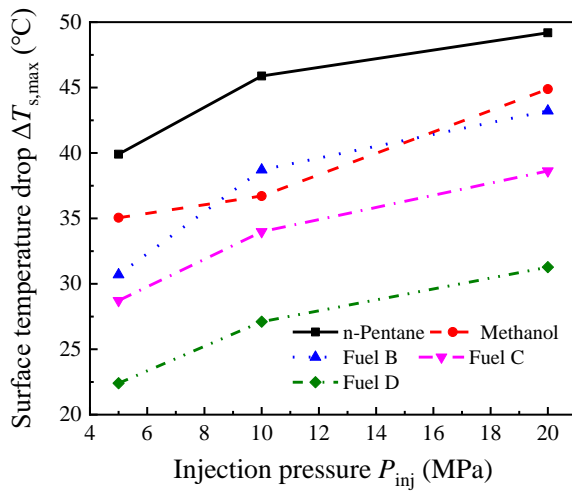


(a) surface temperature

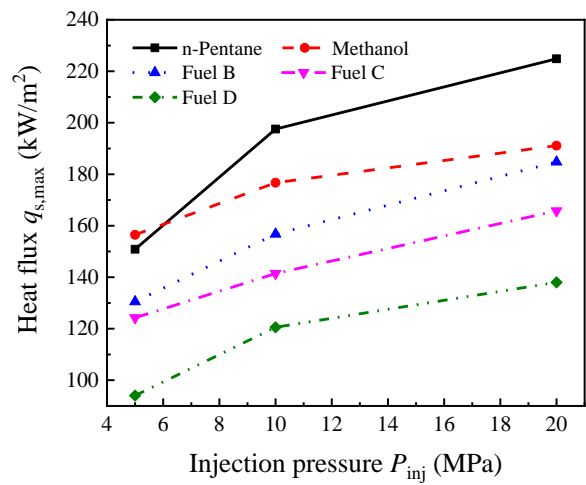


(b) heat flux

Fig.11 Variation of (a) surface temperature and (b) heat flux as a function of time at the condition of $P_{inj}=20$ MPa, $D_{inj}=50$ mm, $T_{pis}=90$ °C, $T_{inj}=50$ °C



(a) maximum surface temperature drop



(b) peak heat flux

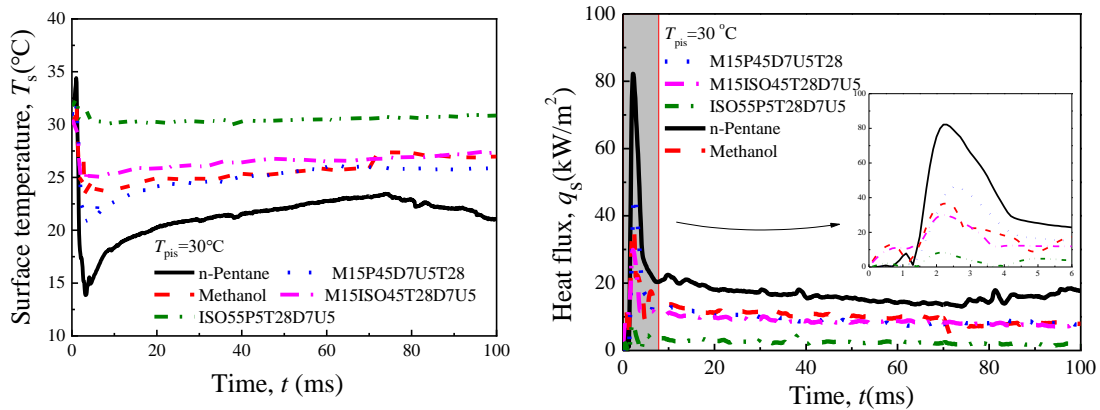
Fig.12 Variations of (a) maximum surface temperature drop ($\Delta T_{s, \max}$) and (b) peak heat flux (q_{\max}) with injection

pressure at the condition of $D_{inj}=50$ mm, $T_{pis}=90$ °C and $T_{inj}=50$ °C

3.2.3 Effect of piston temperature

The influence of piston surface temperatures (low $T_{pis}=30$ °C and high $T_{pis}=90$ °C) on transient surface temperature and heat flux variations with time at conditions of $P_{inj}=10$ MPa, $T_{inj}=50$ °C and $D_{inj}=50$ mm are shown in Fig. 13 and Fig. 14. A higher piston surface temperature makes both the surface temperature drop and the heat flux larger due to the larger temperature difference which enhances the heat transfer intensity.

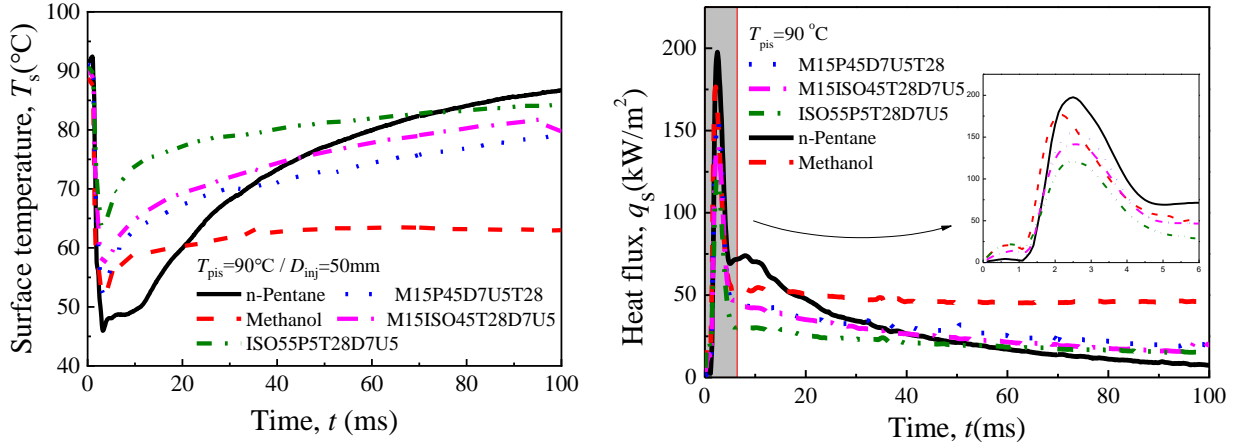
To better illustrate the sensitivity of the heat transfer with the different fuels to the change of piston surface temperature, Fig. 15 shows the variations of the $\Delta T_{s, \max}$ and q_{\max} for the 5 fuels at different piston temperatures. $\Delta T_{s, \max}$ and q_{\max} present a monotonic increase with T_{pis} due to the increasing temperature difference. When T_{pis} is lower than the injection temperature ($T_{pis}=30$ °C), the piston surface temperature by Fuel D has a bit increase rather than decrease as other fuels. This is because fuel D has the highest boiling point of 93.06 °C - far larger than T_{inj} of 50 °C. Droplets of fuel D are most difficult to evaporate due to its poor volatility at low T_{inj} , as a result, the droplets' temperature is still higher than the piston surface temperature, not cooling but heating the piston surface. In the case of a high piston surface temperature (above the injection temperature), the piston surface can be fully cooled, and this causes an increase in $\Delta T_{s, \max}$ and q_{\max} due to the strong cooling. Fuels present different cooling intensities on the piston surface, dependent on the boiling point and enthalpy of vaporization. The boiling point determines the difficulty and extent of fuel vaporization, while enthalpy governs how much heat is absorbed from piston surface once boiling occurs. As can be seen from Fig. 15 (b), n-pentane causes the largest $\Delta T_{s, \max}$ and q_{\max} , probably attributable to the largest temperature difference between the droplets and piston surface due to it having the lowest boiling point. Methanol produces the second largest q_{\max} mainly because of having the highest enthalpy of vaporization. The methanol is followed by fuel B and fuel C. Fuel D possesses the lowest $\Delta T_{s, \max}$ and q_{\max} as expected, due to its low volatility and smallest latent heat.



(a) surface temperature

(b) heat flux

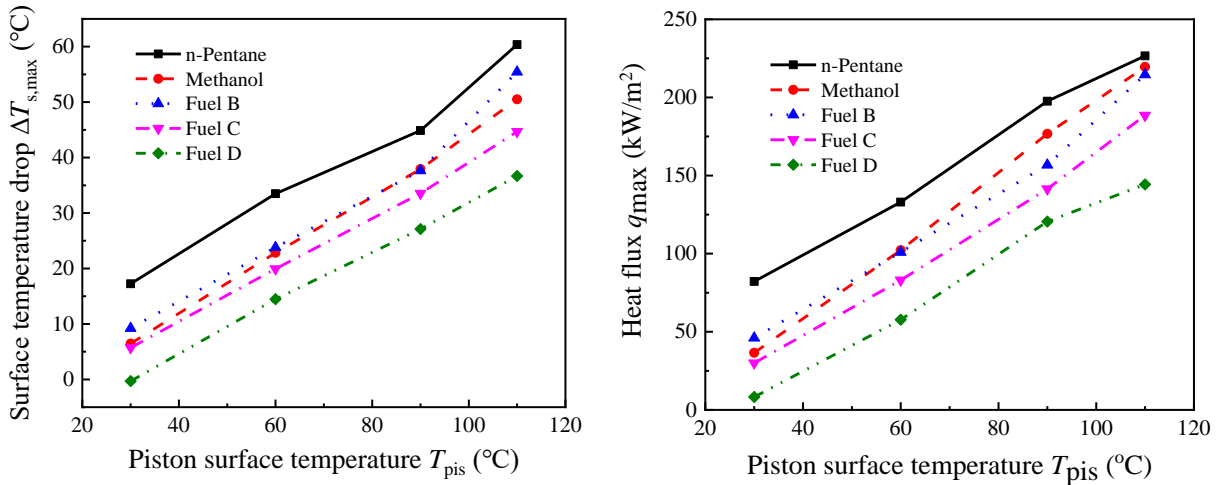
Fig.13 Variation of (a) surface temperature and (b) heat flux as a function of time at the condition of $P_{inj}=10$ MPa, $D_{inj}=50$ mm, $T_{pis}=30$ °C, $T_{inj}=50$ °C



(a) surface temperature

(b) heat flux

Fig.14 Variation of (a) surface temperature and (b) heat flux as a function of time at the condition of $P_{inj}=10$ MPa, $D_{inj}=50$ mm, $T_{pis}=90$ °C, $T_{inj}=50$ °C



(a) peak surface temperature drop

(b) peak heat flux

Fig.15 Variations of (a) maximum surface temperature drop ($\Delta T_{s,max}$) and (b) peak heat flux (q_{max}) with piston temperature at the condition of $P_{inj}=10$ MPa, $T_{inj}=50$ °C and $D_{inj}=50$ mm

3.2.4 Effect of injection distance

Fig. 14 and Fig. 16 show the changes of surface temperature and heat flux with time at two different injection distances ($D_{inj}=50$ mm and 70 mm) when $P_{inj}=10$ MPa, $T_{pis}=90$ °C and $T_{inj}=50$ °C. It is found that the transient heat transfer due to spray impingement with different fuels show different trends as D_{inj} varies from 50 to 70 mm. Generally, for Fuel B, Fuel C, methanol and n-pentane, it is obvious that the spray will have evaporated more and have smaller droplets at the larger distance – causing less

cooling. This is because for these fuels, the liquid temperature will reduce when it emerges into the cold air and potentially below the air temperature but when volatile components leave, it will then warm back up again – more so the further it travels. However, Fuel D is so much less volatile, it is definitely still cooling at both 50 mm and 70 mm and, so it reaches a lower temperature and more cooling capacity at 70 mm.

The sensitivity of heat transfer caused by fuel spray impingement to injection distance is illustrated more clearly in Fig. 17, which compares the maximum drop of surface temperature and peak heat flux at 50 and 70 mm for all five fuels. For n-pentane, it undergoes the most obvious decrease in $T_{s, \max}$ and q_{\max} with the increasing injection distance, due to its lowest boiling point and highest volatility. More specifically, longer injection distance leads to smaller droplets diameter and velocity, and even more droplets disappearing because of the longer vaporizing time, which greatly weakens the impingement intensity on the piston surface. Methanol, fuel B and fuel C experience a smaller decrease in $T_{s, \max}$ and q_{\max} compared with n-pentane, because they are more difficult to evaporate completely. It means the droplets size, velocity and quantity are less influenced by the vaporization as reaching the piston surface. However, there is an increase in $T_{s, \max}$ and q_{\max} for fuel D as D_{inj} is increased from 50 to 70 mm. This is mainly attributed to the low front end volatility of the fuel (see Fig. 4) which causes relatively slower droplet evaporation following injection – thereby maintaining droplet size, spray momentum and impingement intensity. The longer vaporizing time available at the longer D_{inj} allows the droplets to reach a lower temperature also, contributing further to the observed increase of $T_{s, \max}$ and q_{\max} on the piston surface.

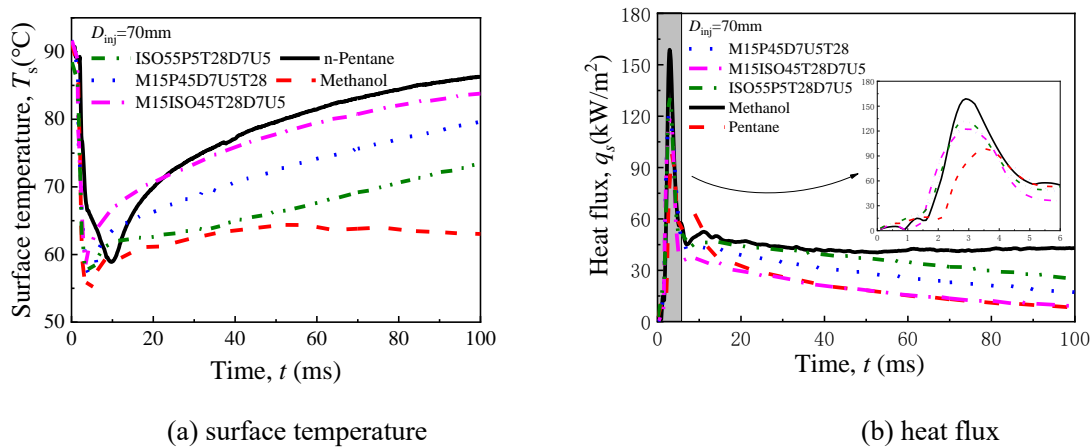
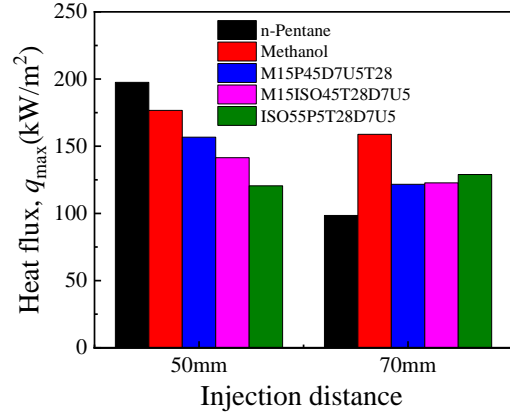
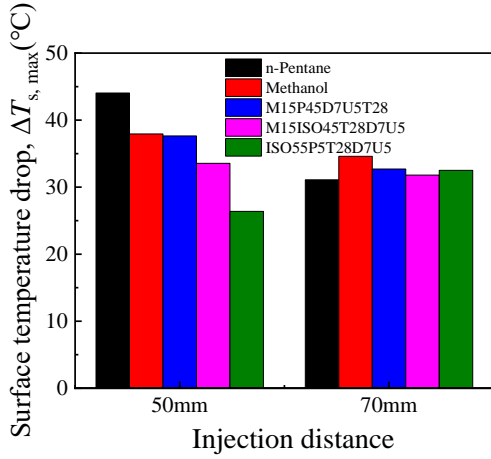


Fig.16 Variation of (a) surface temperature and (b) heat flux as a function of time at the condition of $P_{\text{inj}}=10$ MPa, $D_{\text{inj}}=70$ mm, $T_{\text{pis}}=90$ °C, $T_{\text{inj}}=50$ °C



(a) peak surface temperature drop

(b) peak heat flux

Fig.17 (a) Peak surface temperature drop ($\Delta T_{s, \max}$) and (b) peak heat flux (q_{\max}) at different injection distances

3.2.5 Analysis of peak heat fluxes with P_a/P_{sat} for all fuels

The pressure ratio P_a/P_{sat} is an important value and commonly used to judge the occurrence of flash boiling spray. Fig.18 shows the variation of the peak heat flux as a function of P_a/P_{sat} . All the curves present an exponential variation trend with P_a/P_{sat} . The peak heat flux changes slowly with high P_a/P_{sat} corresponding with low injection temperature (no flash boiling spray) for all fuels, but it starts to decrease dramatically at the point of ~ 0.35 due to the increase in injection temperature. This finding is consistent with the spray image observations that the spray images become more explosive with larger width at the same point of ~ 0.35 . Our findings of the spray and heat transfer behavior coincide with the previous studies by Zeng et al. and Zhang et al. [32, 33] that the non flash-boiling spray transitions to flash-boiling as P_a/P_{sat} is reduced to the region of $0.3 < P_a/P_{\text{sat}} < 1$. An exponential function can be used to describe the q_{\max} variation with P_a/P_{sat} , and its form is as:

$$q_{\max} = a - b \times c^{\frac{P_a}{P_{\text{sat}}}}$$

The three parameters a , b , and c are dependent on fuel property, and their values are shown in Table 2.

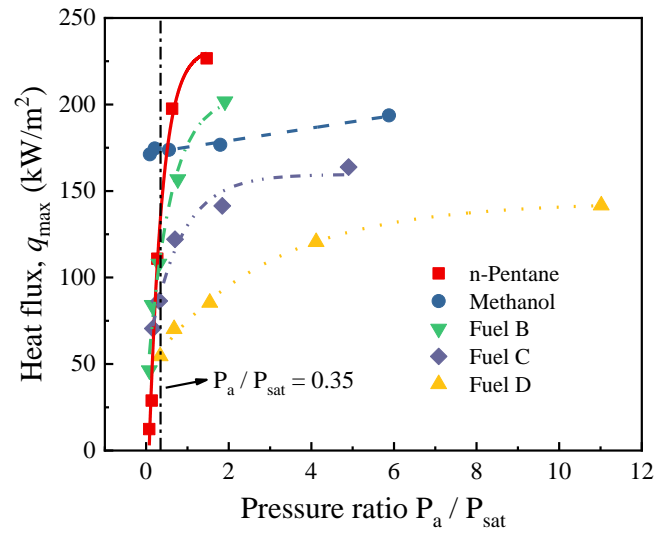


Fig.18 Variation of q_{max} with pressure ratio at condition of $D_{inj}=50$ mm, $P_{inj}=10$ MPa, $T_{pis}=90$ °C

Table 2 The parameters of the fitting equations for the five fuels

Fuel	Best fit parameters in the equation $q_{max} = a - b \times c^{\frac{P_a}{P_{sat}}}$		
	a	b	c
n-pentane	232.59	291.16	0.04
Methanol	136.46	134.74	0.99
Fuel B	205.42	172.96	0.17
Fuel C	159.62	108.53	0.27
Fuel D	143.57	97.71	0.70

4. Conclusions

In this study, an experimental investigation of transient heat transfer induced by the pulsed fuel spray impinging on the piston surface has been conducted. Five fuels with different boiling points and enthalpy of vaporization were designed and tested in the experiments, to investigate fuel property effects - mainly focusing on the volatility on the transient surface temperature and heat flux on the piston at various injection conditions. The main findings are summarized as follows:

Violent flash boiling spray occurs as soon as the ratio of back pressure (atmospheric pressure) to the saturated vapour pressure at the injection temperature is decreased to ~ 0.35 through increasing the injection temperature for different fuels. Further increasing the injection temperature does not enhance spray width and angle but weakens the impinging and cooling intensities on the piston surface due to the strong evaporation of droplets for the high volatility fuels with quite low boiling point and enthalpy of vaporization (such as n-pentane and fuel B). Correspondingly, it leads to a sharp decrease in the maximum surface temperature drop ($\Delta T_{s, max}$) and peak heat flux (q_{max}). On the contrary, increasing the

injection temperature leads to a stronger interaction between the spray and piston surface, and $\Delta T_{s, \max}$ and q_{\max} are far less influenced for the fuels with high enthalpy of vaporization such as methanol and fuel C. This implies that fuels like methanol and C are far more difficult to evaporate once the liquid film forms on the piston surface; this prolongs the liquid film residence time and may be expected to have a negative effect on the combustion efficiency and particulate matter emissions for GDI engines.

The transient heat transfer due to the spray impingement of a particular fuel is insensitive to the changes of injection pressure and piston surface temperature. That is, a fuel with a low initial boiling point and high enthalpy of vaporization always causes a strong cooling intensity on the piston surface with large $T_{s, \max}$ and q_{\max} regardless of the injection pressure and piston surface temperature at the non-flash boiling spray condition.

Fuels present different transient heat transfer performance for the short and long injection distances. At the short distance of 50 mm, the fuels with lower initial boiling point and higher enthalpy of vaporization produce the higher $T_{s, \max}$ and q_{\max} . Increasing the injection distance reduces the $T_{s, \max}$ and q_{\max} to different extents depending on their enthalpy of vaporization - for low initial boiling point fuels (n-pentane, methanol, fuel B and fuel C), while it causes a slight increase in $T_{s, \max}$ and q_{\max} for fuel D with the highest initial boiling point and lowest front end volatility.

Acknowledgement

We sincerely appreciate the great help from Prof. Richard Stone of University of Oxford. We also would like to acknowledge the support from the Ministry of Science and Technology of Shaanxi Province, China (2019KW-021 and 2020KJXX-040). Thanks are also given to the aerospace science funding (2019ZB070002) and the funding (ZQ20195203110) as well as the support from the State Key Laboratory of Engines of Tianjin University (K2019-04).

Conflicts of interest

The authors declare no conflict of interest.

References

- [1] S. Wu, M. Xu, D.L.S. Hung, H. Pan, Effects of nozzle configuration on internal flow and primary jet breakup of flash boiling fuel sprays, *International Journal of Heat and Mass Transfer*, 110 (2017) 730-738.
- [2] T. Ma, L. Feng, H. Wang, H. Liu, M. Yao, Analysis of near wall combustion and pollutant migration after spray impingement, *International Journal of Heat and Mass Transfer*, 141 (2019) 569-579.
- [3] M. Potenza, M. Milanese, A. de Risi, Effect of injection strategies on particulate matter structures of a turbocharged GDI engine, *Fuel*, 237 (2019) 413-428.
- [4] V.C. Raj, P. Kuntikana, S. Sreedhara, S.V. Prabhu, Heat transfer characteristics of impinging methane diffusion and partially premixed flames, *International Journal of Heat and Mass Transfer*, 129 (2019) 873-893.
- [5] Y. Kobashi, Y. Zama, T. Kuboyama, Modeling wall film formation and vaporization of a gasoline

494 surrogate fuel, *International Journal of Heat and Mass Transfer*, 147 (2020) 119035.

495 [6] K. Tong, B.D. Quay, J.V. Zello, D.A. Santavicca, Fuel Volatility Effects on Mixture Preparation
496 and Performance in a GDI Engine During Cold Start, in, SAE International, 2001.

497 [7] M. Chang, Z. Lee, S. Park, S.J.F. Park, Characteristics of flash boiling and its effects on spray
498 behavior in gasoline direct injection injectors: A review, *Fuel*, 271 (2020) 117600.

499 [8] Liu, H., Ma, S., Zhang, Z., Zheng, Yao, M.J.F. Guildford, Study of the control strategies on soot
500 reduction under early-injection conditions on a diesel engine, *Fuel*, 139 (2015) 472-481.

501 [9] M.C. Drake, T.D. Fansler, A.S. Solomon, G. Szekely Jr, Piston fuel films as a source of smoke and
502 hydrocarbon emissions from a wall-controlled spark-ignited direct-injection engine, *SAE transactions*,
503 (2003) 762-783.

504 [10] Y. Li, Y. Huang, S. Yang, K. Luo, R. Chen, C. Tang, A comprehensive experimental investigation
505 on the PFI spray impingement: Effect of impingement geometry, cross-flow and wall temperature,
506 *Applied Thermal Engineering*, 159 (2019) 113848.

507 [11] M. Bovo, L. Davidson, Direct comparison of LES and experiment of a single-pulse impinging jet,
508 *International Journal of Heat and Mass Transfer*, 88 (2015) 102-110.

509 [12] T. Badawy, M.A. Attar, P. Hutchins, H. Xu, J.K. Venus, R. Cracknell, Investigation of injector
510 coking effects on spray characteristic and engine performance in gasoline direct injection engines,
511 *Applied Energy*, 220 (2018) 375-394.

512 [13] Z. Wang, X. Dai, F. Liu, Z. Li, F. Li, Microscopic characterization of spray impingement under
513 flash boiling conditions, *Journal of the Energy Institute*, 92(3) (2019) 640-652.

514 [14] J. Du, B. Mohan, J. Sim, T. Fang, W.L. Roberts, Study of spray collapse phenomenon at flash
515 boiling conditions using simultaneous front and side view imaging, *International Journal of Heat and*
516 *Mass Transfer*, 147 (2020) 118824.

517 [15] J. Serras-Pereira, P. Aleiferis, D. Richardson, Imaging and heat flux measurements of wall
518 impinging sprays of hydrocarbons and alcohols in a direct-injection spark-ignition engine, *Fuel*, 91(1)
519 (2012) 264-297.

520 [16] J. Serras-Pereira, P. Aleiferis, H. Walmsley, T. Davies, R. Cracknell, Heat flux characteristics of
521 spray wall impingement with ethanol, butanol, iso-octane, gasoline and E10 fuels, *International journal*
522 *of heat and fluid flow*, 44 (2013) 662-683.

523 [17] F. Köpple, D. Seboldt, P. Jochmann, A. Hettinger, A. Kufferath, M. Bargende, Experimental
524 investigation of fuel impingement and spray-cooling on the piston of a GDI engine via instantaneous
525 surface temperature measurements, *SAE International Journal of Engines*, 7(3) (2014) 1178-1194.

526 [18] L.K.-L. Shih, T.-C. Hsu, W.-L. Chang, The study of spray impingement on a heated metal plate
527 inside a low-speed wind tunnel, *Journal of the Chinese Institute of Engineers*, 34(3) (2011) 357-366.

528 [19] G. Lepperhoff, M. Houben, Mechanisms of deposit formation in internal combustion engines and
529 heat exchangers, 0148-7191, SAE Technical Paper, 1993.

530 [20] W.-D. Hsieh, J.-H. Lu, R.-H. Chen, T.-H. Lin, Deposit formation characteristics of gasoline spray
531 in a stagnation-point flame, *Combustion and flame*, 156(10) (2009) 1909-1916.

532 [21] Q. Tang, H. Liu, M. Li, M. Yao, Optical study of spray-wall impingement impact on early-
533 injection gasoline partially premixed combustion at low engine load, *Applied Energy*, 185 (2017) 708-
534 719.

535 [22] B. Liang, Y. Ge, J. Tan, X. Han, L. Gao, L. Hao, W. Ye, P. Dai, Comparison of PM emissions from

a gasoline direct injected (GDI) vehicle and a port fuel injected (PFI) vehicle measured by electrical low pressure impactor (ELPI) with two fuels: Gasoline and M15 methanol gasoline, *Journal of Aerosol Science*, 57 (2013) 22-31.

[23] H. Liu, X. Wang, D. Zhang, F. Dong, X. Liu, Y. Yang, H. Huang, Y. Wang, Q. Wang, Z. Zheng, Investigation on blending effects of gasoline fuel with N-butanol, DMF, and ethanol on the fuel consumption and harmful emissions in a GDI vehicle, *Energies*, 12(10) (2019) 1845.

[24] P.G. Aleiferis, Z. Van Romunde, An analysis of spray development with iso-octane, n-pentane, gasoline, ethanol and n-butanol from a multi-hole injector under hot fuel conditions, *Fuel*, 105 (2013) 143-168.

[25] Y. Qian, J. Wang, Z. Li, C. Jiang, Z. He, L. Yu, X. Lu, Improvement of combustion performance and emissions in a gasoline direct injection (GDI) engine by modulation of fuel volatility, *Fuel*, 268 (2020) 117369.

[26] B.A. Vanderwege, S. Hochgreb, The effect of fuel volatility on sprays from high-pressure swirl injectors, in: *Symposium (international) on combustion*, Elsevier Science, 1998, pp. 1865-1871.

[27] K. Tong, B.D. Quay, J.V. Zello, D.A. Santavicca, Fuel volatility effects on mixture preparation and performance in a GDI engine during cold start, *SAE Transactions*, (2001) 2301-2318.

[28] Z.-F. Zhou, S.H.M. Murad, J.-M. Tian, J. Camm, R. Stone, Experimental investigation on heat transfer of n-pentane spray impingement on piston surface, *Applied Thermal Engineering*, 138 (2018) 197-206.

[29] J.-m. Tian, B. Chen, Z.-f. Zhou, Methodology of surface heat flux estimation for 2D multi-layer mediums, *International Journal of Heat and Mass Transfer*, 114 (2017) 675-687.

[30] S.H.M. Murad, J. Camm, M. Davy, R. Stone, D. Richardson, Spray Behaviour and Particulate Matter Emissions with M15 Methanol/Gasoline Blends in a GDI Engine, in: *Sae World Congress & Exhibition*, 2016.

[31] Z. Shi, C.F. Lee, H. Wu, H. Li, F. Liu, Effect of injection pressure on the impinging spray and ignition characteristics of the heavy-duty diesel engine under low-temperature conditions, *Applied Energy*, 262 (2020) 114552.

[32] W. Zeng, M. Xu, G. Zhang, Y. Zhang, D.J.J.F. Cleary, Atomization and vaporization for flash-boiling multi-hole sprays with alcohol fuels, *Fuel*, 95 (2012) 287-297.

[33] G. Zhang, D.L. Hung, M. Xu, Experimental study of flash boiling spray vaporization through quantitative vapor concentration and liquid temperature measurements, *Experiments in fluids*, 55(8) (2014) 1804.

[34] H. Guo, X. Ma, Y. Li, S. Liang, Z. Wang, H. Xu, J. Wang, Effect of flash boiling on microscopic and macroscopic spray characteristics in optical GDI engine, *Fuel*, 190 (2017) 79-89.

[35] Y. Li, H. Guo, Z. Zhou, Z. Zhang, X. Ma, L. Chen, Spray morphology transformation of propane, n-hexane and iso-octane under flash-boiling conditions, *Fuel*, 236 (2019) 677-685.